Author/s:
Bi, PQ;Hall, CR;Yin, H;So, SK;Smith, TA;Ghiggino, KP;Hao, XT

Title:
Resolving the Mechanisms of Photocurrent Improvement in Ternary Organic Solar Cells

Date:
2019-08-01

Citation:
Bi, P. Q., Hall, C. R., Yin, H., So, S. K., Smith, T. A., Ghiggino, K. P. & Hao, X. T. (2019). Resolving the Mechanisms of Photocurrent Improvement in Ternary Organic Solar Cells. Journal of Physical Chemistry C, 123 (30), pp.18294-18302. https://doi.org/10.1021/acs.jpcc.9b06267.

Persistent Link:
https://hdl.handle.net/11343/345175

THE JOURNAL OF PHYSICAL CHEMISTRY C

C: Energy Conversion and Storage; Energy and Charge Transport

Resolving the Mechanisms of Photocurrent Improvement in Ternary Organic Solar Cells

Peng-Qing Bi, Christopher R. Hall, Hang Yin, Shu Kong So, Trevor A. Smith, Kenneth P. Ghiggino, and Xiao-Tao Hao

J. Phys. Chem. C, **Just Accepted Manuscript** • DOI: 10.1021/acs.jpcc.9b06267 • Publication Date (Web): 12 Jul 2019

is published by the American Chemical Society. 1155 Sixteenth Street N.W., Washington, DC 20036

Resolving the Mechanisms of Photocurrent Improvement in Ternary Organic Solar Cells

Peng Qing Bi [†], Christopher R. Hall[‡], Hang Yin[§], Shu Kong So[§], Trevor A. Smith[‡], Kenneth P. Ghiggino[‡], Xiao Tao Hao, [†,‡,*]

[†]School of Physics, State Key Laboratory of Crystal Materials, Shandong University, Jinan, Shandong 250100, China
[‡]ARC Centre of Excellence in Exciton Science, School of Chemistry, The University of Melbourne, Parkville, Victoria 3010, Australia
[§]Department of Physics and Institute of Advanced Materials, Hong Kong Baptist University, Kowloon Tong, Hong Kong 999077, P. R. China

Abstract: The ultra-low band-gap small molecule IEICO-4F has been employed as a

secondary acceptor in both fullerene (PTB7-Th:$PC_{71}BM$) and non-fullerene (PBDB-T:ITIC) based ternary organic solar cells (OSCs). Structural characterization methods combined with ultrafast spectroscopy have been applied to resolve the mechanisms leading to the observed improvement in device efficiency upon addition of IEICO-4F. It is shown that IEICO-4F forms ternary mixed domains in the host systems and improves device efficiency by broadening the absorption spectral range and enhancing both charge separation and charge transport. The enhanced crystallinity of the semiconductor polymer electron donors in the presence of the EIECO-4 provides additional channels for ultrafast charge transfer and transport compared to binary systems. The optimum ternary blend formulations required to improve device efficiencies are reported. This work provides new insights for fabricating high performance ternary OSCs.

INTRODUCTION

Charge recombination, including geminate and non-geminate recombination, is a limiting factor in the performance of organic solar cells (OSCs).[1-3] Charge recombination reduces short-circuit current density (J_{SC}), which constitutes one of the important criteria for high-performance OSCs. The power conversion efficiency (PCE) is also affected by charge recombination as it is determined by J_{SC}, the open circuit voltage (V_{OC}), and the fill factor (FF) as follows (Equation 1):

$$\mathrm{PCE} = \frac{J_{SC} \times V_{OC} \times FF}{P_{in}} \times 100\% \quad (1)$$

where P_{in} represents the incident light power AM 1.5G. Therefore, it is important that charge recombination must be minimized for preparing OSCs with both high J_{SC} and PCE while exploiting their inherent advantages, e.g. light-weight, cost-effectiveness, solution processability, and production by roll-to-roll printing method.[4-9] Several strategies have been developed for reducing charge recombination, including the design of new materials and novel device structures.[10-21] As a result of these efforts, PCEs >11% have been reported for small molecular and polymer-based OSCs [22-26] while PCEs >16% are found for non-fullerene-based OSCs,[27-29] in particular a PCE >17% has been obtained for a tandem OSC.[30]

A single active layer comprising a donor and acceptor limits absorption of the full range of the solar spectrum due to the intrinsic absorption properties of organic materials and this also imposes limitations on PCE improvement.[31-32] However, a ternary structure with two electron donors (acceptors) and one electron acceptor (donor) in a single bulk heterojunction (BHJ) OSC has been shown to be an effective and simple strategy for enhancing or broadening the device absorption spectrum and

subsequently increasing the J_{SC} and PCE of corresponding binary OSCs. Ultra-low band-gap small molecular acceptors have been designed and synthesized to enhance the absorption of OSCs in the near-infrared (NIR) region leading to reported high J_{SC} values in devices.[33-36] These materials thus provide useful third components for extending the absorption spectra of binary systems to the NIR region.

In this study, we report two ternary OSCs based on poly[[2,6′-4,8-di(5-ethylhexylthienyl)benzo[1,2-b;3,3-b]dithiophene][3-fluoro-2[(2-ethylhexyl)carbonyl]thieno[3,4-b]thiophenediyl]]:phenyl-C71-butyric-acid-methylester (PTB7-Th:$PC_{71}BM$) and poly[(2,6-(4,8-bis(5-(2-ethylhexyl)thiophen-2-yl)benzo[1,2-b:4,5-b′]dithiophene)-co-(1,3-di(5-thiophene-2-yl)-5,7-bis(2-ethylhexyl)benzo[1,2-c:4,5-c′]dithiophene-4,8-dione)]:3,9-bis(2-methylene-(3-(1,1-dicyanomethylene)-indanone)-5,5,11,11-tetrakis(4-hexylphenyl)-dithieno[2,3-d:2′,3′-d′]-s-indaceno[1,2-b:5,6-b′]-dithiophene (PBDB-T:ITIC) with an ultra-low band-gap small molecule 2,2′-((2Z,2′Z)-(((4,4,9,9-tetrakis(4-hexylphenyl)-4,9-dihydro-s-indaceno[1,2-b:5,6-b′]dithiophene-2,7-diyl)bis(4-((2-ethylhexyl)oxy)thiophene-5,2-diyl))bis(methanylylidene))bis(5,6-difluoro-3-oxo-2,3-dihydro-1H-indene-2,1-diylidene))dimalononitrile (IEICO-4F) as the third component. Nanomorphology studies as well as electrical and optical measurements, have been carried out to characterize the effects of IEICO-4F in the ternary blends. This approach revealed that the IEICO-4F in the ternary blends suppresses charge recombination, facilitates charge transfer and increases the

efficiency of charge transport. The J_{SC} of both binary devices is clearly boosted by the third component.

EXPERIMENTAL SECTION

Materials. PTB7-Th, $PC_{71}BM$, PBDB-T and ITIC and IEICO-4F were purchased from Solarmer Materials, Inc. All of the materials were used as received without further purification.

Materials Characterization. Absorption spectra were obtained using an ultraviolet-visible (*UV-vis*) dual beam spectrophotometer (TU-1900, PG Instruments, Ltd.). Steady-state photoluminescence (PL) spectra were collected by a spectrometer (DU420A-OE, ANDOR), the excitation wavelength was 500 nm. Atomic force microscopy (AFM) with tapping mode (Solver P47 PRO, NTMDT Co.) was used to study the nanomorphology of the films. Time-resolved photoluminescence (TRPL) profiles were collected by a Nanofinder FLEX2 (Tokyo Instruments, Inc.) microscope attached with a TCSPC module (Becker & Hickl, SPC-150). Grazing-incidence wide-angle X-ray scattering (GIWAXS) was performed at the BL16B1 beamline of the Shanghai Synchrotron Radiation Facility. The wavelength of the incident X-ray beam was 0.124 nm and sample-to-detector distance was 200 mm. The incidence light angle was 0.12° and a mar165CCD was used to collect the scattering signal. All of the samples used for GIWAXS measurements were prepared by spin-coating the blend solutions onto Si wafers.

GISAXS Modeling. 1D GISAXS profiles were fitted by the fitting software SasView. Debye-Anderson-Brumberger (DAB) was used to study the domain size

and phase distribution of the third component in ternary blends in the low-q range up to 0.008 Å^{-1},

$$\mathrm{I}(q) = \frac{A1}{[1 + (q\xi)2]2}$$

where q is the scattering wave vector, A_1 is an independent fitting parameter, and ξ is the average correlation length of the acceptor dispersed polymer domain.

For the transient absorption spectroscopy (TAS) measurements, the pump beam was generated by a high repetition rate Ti:sapphire regenerative amplifier system (Coherent RegA9050, centered at 800 nm, 92 kHz) pumping an optical parametric amplifier (Coherent 9450). The supercontinuum broadband near-infrared probe light source was generated by focusing the residual 800 nm beam to a 3 mm uncoated undoped YAG window (CRYSTECH). The pump beam was mechanically chopped to 4.6 kHz. The pulse energy was less than 30 nJ in order to eliminate any multiexciton effects. The transmitted probe beam was detected using a NIR spectrometer system (Ultrafast Systems, 7200 spectra/sec) synchronized to the excitation pulses and chopper.

Fabrication and Characterization of the OSCs. Inverted structure was adopted for device fabrication. Indium tin oxide (ITO)-coated glass plates (~15 Ω sq^{-1}) were cleaned by ultrasonic treatment in detergent, acetone, and isopropanol, respectively. The ITO glass substrates were then treated with ultraviolet-ozone for 15 min. Zinc oxide (ZnO) precursor solution obtained by dissolving 0.14 g of zinc acetate dihydrate ($Zn(CH_3COO)_2•2H_2O$) and 0.5 g of ethanolamine ($NH_2CH_2CH_2OH$) in 5 ml of 2-methoxyethanol ($CH_3OCH_2CH_2OH$), was spin coated on the ITO substrates at 3000

revolutions per minute (rpm). The ZnO precursor solution-coated substrates were then baked in air at 200°C for 1h immediately. Active layers (~100 nm) were obtained by spin-coating the blend solutions of PTB7-Th:IEICO-4F:$PC_{71}BM$ (10 mg ml^{-1} for donor and 15 mg ml^{-1} for acceptor in chlorobenzene), PBDB-T:IEICO-4F:ITIC blend solutions (10 mg ml^{-1} for donor and 10 mg ml^{-1} for acceptor in chlorobenzene) with solvent additives (1% 1,8-diiodooctane (DIO)) on the ZnO layers. For the PBDB-T:ITIC system, the blend films were annealed on a hot plate at 130°C for 30 min. Finally, 10 nm MoO_3 and 100 nm Ag were deposited on the active layers at a pressure of 1.5×10^{-6} Torr. The effective area of the device is 4 mm^2. The fabrication processes of electron-only and hole-only devices were similar with the OSC devices. A structure of ITO/PEDOT:PSS/active layers/spiro-TPD:CuPc/Au was used to fabricate the hole-only device, and the structure of the electron-only device was ITO/Al/Active layers/LiF/Al. Current density-voltage (*J-V*) characteristics of the OSCs were measured under AM1.5G illumination of 100 mW cm^{-2} (2400, Keithley Instruments Inc., Cleveland, OH, USA). The external quantum efficiency (EQE) was characterized by a 7-SCSpec system (SOFN INSTRUMENTS CO., LTD).

RESULTS AND DISCUSSION

Material Properties. Figure 1a shows the chemical structures of all materials used in the active layers. Figure 1b, c, d shows the steady-state *UV–vis* absorption spectra of neat and blend films. Notably, IEICO-4F exhibits a strong absorption in the region 600-1000 nm. The binary blends of PTB7-Th:$PC_{71}BM$ and PBDB-T:ITIC exhibit absorption spectra that cover the entire visible region, which was further

extended to the NIR region (~1000 nm) by the addition of IEICO-4F, thus maximizing the solar photons utilized.

Device Performance. Ternary OSCs with an inverted structure were fabricated to investigate the effects of IEICO-4F on the performance of binary OSCs. Figure 2a, b shows the *J-V* curves of ternary OSCs based on PTB7-Th:$PC_{71}BM$ and PBDB-T:ITIC with different IEICO-4F weight ratios, respectively. Table 1 summarizes the detailed parameters. A binary OSC based on PTB7-Th:$PC_{71}BM$ exhibited a maximum PCE of 9.16% with a J_{SC} of 17.39 mA cm^{-2}, a V_{OC} of 0.80 V, and a *FF* of 65%. The binary OSC based on PBDB-T:ITIC exhibited a maximum PCE of 9.26%, with J_{SC}, V_{OC}, and *FF* values of 17.13 mA cm^{-2}, 0.87 V, and 62%, respectively. For the optimized ternary OSC based on PTB7-Th:$PC_{71}BM$ with 30 wt% of IEICO-4F, J_{SC} increased from 17.39 to 22.97 mA cm^{-2}, with a decrease in V_{OC} and *FF* to 0.76 V and 61%, respectively (PCE of 10.43%). Hence, doping with 30 wt% of IEICO-4F leads to a 10.76% increase in the PCE of the PTB7-Th:$PC_{71}BM$-based device. Moreover, the J_{SC} of the OSC based on PTB7-Th:IEICO-4F:30 wt% $PC_{71}BM$ further increased to 23.68 mA cm^{-2} with an optimized DIO content (1.5 vol%). Figure S1 and Table S1 show the *J-V* curves and device parameters of the optimized ternary OSCs based on PTB7-Th:$PC_{71}BM$ with different contents of DIO, respectively. For the PBDB-T:ITIC system, PCE increased from 9.26% to 10.25%, J_{SC} increased to 19.14 mA cm^{-2}, and V_{OC} slightly decreased to 0.86 V. In addition, the changes in the V_{OC} of these two systems were dependent on the IEICO-4F composition. This result is similar to that observed for an 'alloy model' reported previously which described the

distribution of the third component in the host system.[37-39] Figure 2c, d shows the corresponding EQE profiles. The EQE values in range from 800 nm to 1000 nm enhanced obviously, which was contributed to the broadened absorption spectra by the additional IEICO-4F. In addition, the ternary OSCs with 30 wt% IEICO-4F in PTB7-Th: IEICO-4F: $PC_{71}BM$ and 20 wt% IEICO-4F in PBDB-T: IEICO-4F: ITIC have the largest EQE values among the ternary OSCs with various IEICO-4F doping in range from 550 nm to 800 nm, which can be ascribed to the enhanced charge generation and charge transport ability.[40-41]

Charge Transfer. TRPL measurements were carried out to analyze the effects of IEICO-4F on the transfer of charge at the interface between the donor and acceptor. Figure 3a, b shows the fluorescence decay kinetics of the donors in neat, binary, and ternary films. Figure S2 shows the normalized PL spectra of the neat films and fluorescence decay kinetics of ITIC in neat and blend films. Table S2 summarizes the detailed decay kinetic parameters. The amplitude weighted average fluorescence decay times of PTB7-Th and PTB7-Th:$PC_{71}BM$ blend films were 127 and 63 ps, respectively. Moreover, after doping the binary film with 30 wt% IEICO-4F, the average fluorescence decay time further decreased to 46 ps. The decrease in emission lifetime can be related to more efficient exciton dissociation ($E = {\tau_{blend}}/{\tau_d}$).[42] τ_d, the dissociation lifetime, can be calculated using Equation 2.

$$\tau_d = \left(\tau_{blend}^{-1} - \tau_{neat}^{-1}\right)^{-1} \quad (2)$$

where τ_{blend} and τ_{neat} represent the average fluorescence lifetimes of the blend and neat films, respectively. Approximately 50% of the photoinduced excitons dissociated

into free charges (Equation 2) and by doping with 30 wt% IEICO-4F, the dissociation percentage increased to 75%. The enhanced dissociation rate in turn led to the observed increase in the J_{SC} of binary OSCs. Similar behavior was observed for the PBDB-T:ITIC-based ternary blends. The amplitude weighted average fluorescence decay times of PBDB-T and PBDB-T:ITIC blend films were 317 and 30 ps, respectively. Moreover, after doping the binary film with 20 wt% IEICO-4F, the average fluorescence decay time further decreased to 25 ps. A high exciton dissociation percentage of 90% was observed for the PBDB-T:ITIC blends, which may be related to the presence of a large interface between the donor and acceptor. However, after doping with 20 wt% of IEICO-4F, the exciton dissociation percentage increased to 92%, which was partially related to the increased J_{SC} of the ternary device. IEICO-4F in the ternary blend BHJ is confirmed to enhance charge transfer, thereby leading to decreased exciton recombination and increased J_{SC}.

Nanomorphology Properties. GIWAXS and AFM (Figure S3 and S4) were used to study the nanomorphology of the films. GIWAXS is a versatile technique for detecting the nanostructure and crystallite orientation of thin films. In this study, this technique was employed to examine the effects of IEICO-4F on the molecular crystallinity and orientation of host donors and acceptors. Figure 4a, b, c, d, e, f and Figure S5 show the 2D GIWAXS patterns. The corresponding profiles are show in Figure 4g, h. Table S3 summarizes the detailed parameters of crystallinity. The (100) lamellar structure peaks and (010) π-π stacking peaks in the out-of-plane direction were observed for all neat films except $PC_{71}BM$, indicative of the dominant face-on

orientation; this orientation also ensured better compatibility between the materials.[43-44] The (010) π-π stacking peak for the neat PTB7-Th film was observed at 16.48 nm^{-1}, with a corresponding *d*-spacing (*d*) of 0.38 nm ($d = 2\pi/q$) for π-π stacking. Moreover, the coherence length (CL) for π-π stacking can be calculated using Equation 3.

$$\mathrm{CL} = 2\pi k/\Delta q \quad (3)$$

where Δq is the full-width at half-maximum (FWHM) for the π-π stacking peak. *K* is the Scherrer constant, which has a value about 1 in block copolymers and surfactant mesophases.[43] The CL of PTB7-Th in the PTB7-Th:$PC_{71}BM$ blend film was 3.03 nm. Furthermore, with the addition of 30 wt% IEICO-4F, the CL of PTB7-Th in the ternary blends increased to 4.39 nm, which was beneficial for charge transport. In addition, the crystalline characteristics of the IEICO-4F neat film and IEICO-4F in the ternary systems were examined. For the IEICO-4F neat film, the (010) peak was observed at 18.76 nm^{-1}, corresponding to a π-π stacking distance of 0.33 nm and a CL of 2.71 nm. Notably, the IEICO-4F crystallites in the ternary blends preferentially exhibited a higher scattering intensity, and decreased FWHM of the (010) peaks for IEICO-4F (Table S3). This phenomenon was similar to that reported for the alloy model proposed for ternary blends in the study by Wei et al.,[39] which further confirmed that the third component distributed in the host systems. In addition, the crystallinity of PBDB-T and IEICO-4F can be mutually promoted in the presence of IEICO-4F in the ternary blends. With a 20 wt% doping of IEICO-4F in the PBDB-T:ITIC blends, the CL of PBDB-T increased from 2.66 to 4.10 nm. The CL of

ITIC decreased from 5.6 to 4.07 nm, possibly related to similar acceptor-donor-acceptor chemical structures between IEICO-4F and ITIC enabling IEICO-4F to insert into the ITIC domains. GIWAXS results revealed the crystallinity of IEICO-4F and donors in the ternary blends can be mutually facilitated, which was beneficial for the transport of charges and a decrease in the geminate charge recombination.

GISAXS was further performed to study the phase distribution of the IEICO-4F in both ternary blends and the domain size. 2D GISAX patterns and the corresponding 1D profiles are shown in Figure 5a, b, c, d, e, f and Figure 5g, h, respectively. The profiles were fitted with a universal model which was described in the experimental section.[45] In polymer/small molecule-based blend systems, the scattering intensity in the low-*q* region (0.00327-0.008 $Å^{-1}$) is contributed by the polymer-rich domain. The high-*q* region scattering intensity comes from fractal-like aggregations.[46-48] Compared to the binary systems of PBDB-T:ITIC and PTB7-Th:$PC_{71}BM$, obvious upturns in the low-*q* region (0.004-0.017 $Å^{-1}$) can be seen in the profiles, as shown in Figure 5g, h. According to previous studies, the intensity upturns in the low-*q* region are caused by the crystalline IEICO-4F dispersed in the amorphous PBDB-T:ITIC and PTB7-Th:$PC_{71}BM$ matrixes.[48-50] However, the high-*q* region scattering intensity does not show any significant changes, which means IEICO-4F did not form fractal aggregates. The results are consistent with the GIWAXS studies. The DAB model was used to quantitatively model the scattering of dispersed IEICO-4F within the PBDB-T:ITIC and PTB7-Th:$PC_{71}BM$ domains in the low-*q* range up to 0.008 $Å^{-1}$.

The correlation length (ξ) can be approximately regarded as the size of the amorphous PBDB-T:ITIC and PTB7-Th:$PC_{71}BM$ domains. When introduce IEICO-4F in the binary systems, the domain size of amorphous PBDB-T:ITIC and PTB7-Th:$PC_{71}BM$ (ξ) decreased from 23.0 to 14.7 nm and 30.0 to 12.5 nm respectively. The results suggests that the IEICO-4F dispersed in the PBDB-T:ITIC and PTB7-Th:$PC_{71}BM$ and also leads to a decrease of the large PBDB-T:ITIC and PTB7-Th:$PC_{71}BM$ domains.

Charge Recombination. TAS were carried out to specifically examine the molecular-scale charge generation and recombination properties in these two ternary systems. Figure 6a, b, d, e and Figure S7 show the spectra recorded at greater than 900 nm in which only the photoinduced absorption (PIA) features of the excitons and charges are observed. The PIA peak was observed at ~1150 nm for the PTB7-Th:$PC_{71}BM$ system, corresponding to the hole polaron absorption of PTB7-Th.[51] The hole polaron absorption band in the ternary film was red-shifted (~30 nm) compared to the binary blend films, possibly suggesting that the charge in the ternary blend film is not localized onto single chains but is delocalized over the crystalline phase.[52-53] Figure 6c shows the polaron generation and decay kinetics of PTB7-Th for the binary and ternary systems. The *ΔOD* amplitude of the ternary blends was two times greater than that of the binary blends, indicating that a larger population of free polarons exists in the ternary blends compared to the binary blends. For the PBDB-T:ITIC system, the absorption at 980 nm corresponded to the singlet exciton absorption of ITIC by comparison with the TA data of neat films (Figure S7).

The PIA observed at ~1180 nm was possibly related to the singlet exciton absorption of IEICO-4F. Figure 6f shows the decay dynamics of the singlet excitons, which was more rapid in the ternary system than the corresponding binary blend, indicating that IEICO-4F can enhance the exciton dissociation pathways.

Charge Transport. Hole-only and electron-only devices were fabricated to analyze the charge-transport properties. Figures 7a and c show the *J–V* curves of the hole-only and electron-only devices. The Mott-Gurney law (Equation 4) was used to fit the curves to calculate the charge carrier mobilities, μ.

$$J_{SCL}d = \frac{9}{8}\varepsilon_0\varepsilon_r\mu_0 \exp\left(0.89\beta\sqrt{F}\right)F^2 \quad (4)$$

where J_{SCL} is the space-charge-limited current density, ε_0 is the permittivity of vacuum, ε_r is the relative dielectric constant, β is the Poole-Frenkel slope, F is the applied electric field, and d is the BHJ film thickness.[54] The calculated hole mobilities, μ, of both binary and ternary BHJs do not differ significantly. The electron mobilities for PTB7-TH:$PC_{71}BM$ and PBDB-T:ITIC were 6.43×10^{-4} and 5.95×10^{-5} $cm^2\ V^{-1}\ s^{-1}$, respectively. However, the addition of IEICO-4F led to a significant decrease in the electron mobilities to 1.53×10^{-4} and 1.82×10^{-5} $cm^2\ V^{-1}\ s^{-1}$ for PTB7-Th:$PC_{71}BM$ and PBDB-T:ITIC, respectively. Temperature-dependent *J-V* measurements of hole-only and electron-only devices were carried out to investigate the reason for the decreased electron mobilities. The Gaussian disorder model (GDM) was employed to analyze the low-field mobilities at different temperatures (Figure 7b, d). The low-field electron and hole mobilities were calculated by fitting the profiles according to Equation 5.

$$\mu_0 = \mu_\infty exp\left[-\left(2\sigma/3kT\right)^2\right] \quad (5)$$

where σ represents the energetic disorder; k is the Boltzmann constant; T is the absolute temperature; and μ_∞ is the high-temperature charge mobility. It has previously been suggested that the energy disorder σ is a key parameter for determining charge mobilities and carrier recombination.[55] Figure 7b, d shows the σ values obtained by plotting μ_0 as a function of $1/T^2$. Table 2 summarizes the detailed parameters of σ. For the PTB7-Th:$PC_{71}BM$ system, σ values were similar for electrons (69 ± 3 meV) and holes (80 ± 2 meV), indicating that the decreased mobilities can be mainly attributed to the low mobility of IEICO-4F.[56] After the addition of 30 wt% of IEICO-4F, the σ of the electrons for the binary blends of the non-fullerene system of PBDB-T:ITIC increased from 68 to 86 meV. The increased energy disorder can be related to the formation of trap states, which led to the increased value of σ.

CONCLUSIONS

Two ternary OSCs based on PTB7-Th:$PC_{71}BM$ and PBDB-T:ITIC were investigated using the small molecule acceptor IEICO-4F as the third component. The crystallinity of IEICO-4F and the donors can be mutually promoted in the blends, leading to an increased charge-transfer efficiency and decreased charge recombination. In addition, IEICO-4F broadened the absorption spectra of the binary systems into the IR region. The J_{SC} of the binary OSCs was significantly improved in addition to the slight decrease in the *FF*, which may be attributed the low charge mobility of IEICO-4F. High PCEs of 11.4% and 10.5% for the PTB7-Th:$PC_{71}BM$ and the

PBDB-T:ITIC systems with IEICO-4F are obtained, indicating that IEICO-4F is an extremely useful component for preparing high-performance ternary OSCs.

■ ASSOCIATED CONTENT

Supporting Information

The Supporting Information is available free of charge on the ACS Publications website at DOI: xxx

J–V curves; PL spectra; Fluorescence decay kinetics; AFM images and RMS of AFM images; 2D GIWAXS patterns; TA spectra; Ternary OSC properties; Fluorescence decay parameters; GIWAXS parameters.

■ AUTHOR INFORMATION

Corresponding Author
*E-mail: haoxt@sdu.edu.cn

Notes

The authors declare no competing financial interests.

■ ACKNOWLEDGEMENTS

This work was supported by the National Natural Science Foundation of China (61631166001). S.K.S would like to acknowledge support from the Research Grant Council of Hong Kong under Grant # N_HKBU202/16. Support from the University of Melbourne International Research and Research Training Fund (IRRTF) and the ARC Centre of Excellence in Exciton Science (CE170100026) are acknowledged. The authors would like to thank the Shanghai Synchrotron Radiation Facility (beam line BL16B1) for providing the beam time for GIXS measurements.

■ REFERENCES

1. Günes, S.; Neugebauer, H.; Sariciftci, N. S., Conjugated Polymer-Based Organic Solar Cells. *Chem. Rev.* **2007,** *107*, 1324-1338.
2. Benduhn, J.; Tvingstedt, K.; Piersimoni, F.; Ullbrich, S.; Fan, Y.; Tropiano, M.; McGarry, K. A.; Zeika, O.; Riede, M. K.; Douglas, C. J. et al., Intrinsic non-Radiative Voltage Losses in Fullerene-Based Organic Solar Cells. *Nat. Energy* **2017,** *2*, 17053.
3. Menke, S. M.; Ran, N. A.; Bazan, G. C.; Friend, R. H., Understanding Energy Loss in Organic Solar Cells: Toward a New Efficiency Regime. *Joule* **2018,** *2*, 25-35.
4. Heeger, A. J., 25th Anniversary Article: Bulk Heterojunction Solar Cells: Understanding the Mechanism of Operation. *Adv. Mater.* **2014,** *26*, 10-28.
5. Xie, Y.; Yang, F.; Li, Y.; Uddin, M. A.; Bi, P.; Fan, B.; Cai, Y.; Hao, X.; Woo, H. Y.; Li, W. et al., Morphology Control Enables Efficient Ternary Organic Solar Cells. *Adv. Mater.* **2018,** *30*, 1803045.
6. Xie, Y.; Huo, L.; Fan, B.; Fu, H.; Cai, Y.; Zhang, L.; Li, Z.; Wang, Y.; Ma, W.; Chen, Y. et al., High-Performance Semitransparent Ternary Organic Solar Cells. *Adv. Funct. Mater.* **2018,** *28*, 1800627.
7. Espinosa, N.; Hösel, M.; Jørgensen, M.; Krebs, F. C., Large Scale Deployment of Polymer Solar Cells on Land, on Sea and in the Air. *Energy Environ. Sci.* **2014,** *7*, 855-866.
8. Jensen, J.; Hösel, M.; Dyer, A. L.; Krebs, F. C., Development and Manufacture of Polymer-Based Electrochromic Devices. *Adv. Funct. Mater.* **2015,** *25*, 2073-2090.
9. Thompson, B. C.; Fréchet, J. M. J., Polymer–Fullerene Composite Solar Cells. *Angew. Chem. Int. Ed. Engl.* **2008,** *47*, 58-77.
10. Brabec, C. J.; Heeney, M.; McCulloch, I.; Nelson, J., Influence of Blend Microstructure on Bulk Heterojunction Organic Photovoltaic Performance. *Chem. Soc. Rev.* **2011,** *40*, 1185-1199.
11. Cao, W.; Xue, J., Recent Progress in Organic Photovoltaics: Device Architecture and Optical Design. *Energy Environ. Sci.* **2014,** *7*, 2123-2144.
12. Duan, C.; Zhang, K.; Zhong, C.; Huang, F.; Cao, Y., Recent Advances in Water/Alcohol-Soluble π-Conjugated Materials: New Materials and Growing Applications in Solar Cells. *Chem. Soc. Rev.* **2013,** *42*, 9071-9104.
13. Lu, L.; Zheng, T.; Wu, Q.; Schneider, A. M.; Zhao, D.; Yu, L., Recent Advances in Bulk Heterojunction Polymer Solar Cells. *Chem. Rev.* **2015,** *115*, 12666-12731.
14. Wu, J.-S.; Cheng, S.-W.; Cheng, Y.-J.; Hsu, C.-S., Donor–Acceptor Conjugated Polymers Based on Multifused Ladder-Type Arenes for Organic Solar Cells. *Chem. Soc. Rev.* **2015,** *44*, 1113-1154.
15. Ye, L.; Zhang, S.; Huo, L.; Zhang, M.; Hou, J., Molecular Design toward Highly Efficient Photovoltaic Polymers Based on Two-Dimensional Conjugated Benzodithiophene. *Acc. Chem. Res.* **2014,** *47*, 1595-1603.
16. Yip, H.-L.; Jen, A. K. Y., Recent Advances in Solution-Processed Interfacial Materials for Efficient and Stable Polymer Solar Cells. *Energy Environ. Sci.* **2012,** *5*, 5994-6011.
17. Zhao, X.; Zhan, X., Electron Transporting Semiconducting Polymers in Organic Electronics. *Chem. Soc. Rev.* **2011,** *40*, 3728-3743.
18. Liang, Y.; Wu, Y.; Feng, D.; Tsai, S.-T.; Son, H.-J.; Li, G.; Yu, L., Development of New Semiconducting Polymers for High Performance Solar Cells. *J. Am. Chem. Soc.* **2009,** *131*, 56-57.
19. Cheng, Y.-J.; Yang, S.-H.; Hsu, C.-S., Synthesis of Conjugated Polymers for Organic Solar Cell

Applications. *Chem. Rev.* **2009,** *109*, 5868-5923.

20. Li, Y., Molecular Design of Photovoltaic Materials for Polymer Solar Cells: Toward Suitable Electronic Energy Levels and Broad Absorption. *Acc. Chem. Res.* **2012,** *45*, 723-733.

21. Baran, D.; Gasparini, N.; Wadsworth, A.; Tan, C. H.; Wehbe, N.; Song, X.; Hamid, Z.; Zhang, W.; Neophytou, M.; Kirchartz, T. et al., Robust Nonfullerene Solar Cells Approaching Unity External Quantum Efficiency Enabled by Suppression of Geminate Recombination. *Nat. Commun.* **2018,** *9*, 2059.

22. Chen, C.-C.; Chang, W.-H.; Yoshimura, K.; Ohya, K.; You, J.; Gao, J.; Hong, Z.; Yang, Y., An Efficient Triple-Junction Polymer Solar Cell Having a Power Conversion Efficiency Exceeding 11%. *Adv. Mater.* **2014,** *26*, 5670-5677.

23. Li, S.; Ye, L.; Zhao, W.; Zhang, S.; Mukherjee, S.; Ade, H.; Hou, J., Energy-Level Modulation of Small-Molecule Electron Acceptors to Achieve over 12% Efficiency in Polymer Solar Cells. *Adv. Mater.* **2016,** *28*, 9423-9429.

24. Nian, L.; Gao, K.; Liu, F.; Kan, Y.; Jiang, X.; Liu, L.; Xie, Z.; Peng, X.; Russell, T. P.; Ma, Y., 11% Efficient Ternary Organic Solar Cells with High Composition Tolerance via Integrated Near-IR Sensitization and Interface Engineering. *Adv. Mater.* **2016,** *28*, 8184-8190.

25. Zhao, W.; Li, S.; Yao, H.; Zhang, S.; Zhang, Y.; Yang, B.; Hou, J., Molecular Optimization Enables over 13% Efficiency in Organic Solar Cells. *J. Am. Chem. Soc.* **2017,** *139*, 7148-7151.

26. Li, M.; Gao, K.; Wan, X.; Zhang, Q.; Kan, B.; Xia, R.; Liu, F.; Yang, X.; Feng, H.; Ni, W. et al., Solution-Processed Organic Tandem Solar Cells With Power Conversion Efficiencies >12%. *Nat. Photonics* **2016,** *11*, 85.

27. Yuan, J.; Zhang, Y.; Zhou, L.; Zhang, G.; Yip, H.-L.; Lau, T.-K.; Lu, X.; Zhu, C.; Peng, H.; Johnson, P. A. et al., Single-Junction Organic Solar Cell with over 15% Efficiency Using Fused-Ring Acceptor with Electron-Deficient Core. *Joule* **2019,** *3*, 1140-1151.

28. Fan, B.; Zhang, D.; Li, M.; Zhong, W.; Zeng, Z.; Ying, L.; Huang, F.; Cao, Y., Achieving over 16% Efficiency for Single-Junction Organic Solar Cells. *Sci. China Chem.* **2019,** *62*, 746-752.

29. Cui, Y.; Yao, H.; Hong, L.; Zhang, T.; Xu, Y.; Xian, K.; Gao, B.; Qin, J.; Zhang, J.; Wei, Z. et al., Achieving Over 15% Efficiency in Organic Photovoltaic Cells via Copolymer Design. *Adv. Mater.* **2019,** *31*, 1808356.

30. Meng, L.; Zhang, Y.; Wan, X.; Li, C.; Zhang, X.; Wang, Y.; Ke, X.; Xiao, Z.; Ding, L.; Xia, R. et al., Organic and Solution-Processed Tandem Solar Cells with 17.3% Efficiency. *Science* **2018,** *361*, 1094.

31. Bi, P.; Zheng, F.; Yang, X.; Niu, M.; Feng, L.; Qin, W.; Hao, X., Dual Förster Resonance Energy Transfer Effects in Non-Fullerene Ternary Organic Solar Cells with the Third Component Embedded in the Donor and Acceptor. *J. Mater. Chem. A* **2017,** *5*, 12120-12130.

32. Bi, P.; Xiao, T.; Yang, X.; Niu, M.; Wen, Z.; Zhang, K.; Qin, W.; So, S. K.; Lu, G.; Hao, X. et al., Regulating the Vertical Phase Distribution by Fullerene-Derivative in High Performance Ternary Organic Solar Cells. *Nano Energy* **2018,** *46*, 81-90.

33. Chen, Z.; Cai, P.; Chen, J.; Liu, X.; Zhang, L.; Lan, L.; Peng, J.; Ma, Y.; Cao, Y., Low Band-Gap Conjugated Polymers with Strong Interchain Aggregation and Very High Hole Mobility Towards Highly Efficient Thick-Film Polymer Solar Cells. *Adv. Mater.* **2014,** *26*, 2586-2591.

34. Cui, Y.; Yang, C.; Yao, H.; Zhu, J.; Wang, Y.; Jia, G.; Gao, F.; Hou, J., Efficient Semitransparent Organic Solar Cells with Tunable Color enabled by an Ultralow-Bandgap Nonfullerene Acceptor. *Adv. Mater.* **2017,** *29*, 1703080.

35. Deshmukh, K. D.; Qin, T.; Gallaher, J. K.; Liu, A. C. Y.; Gann, E.; O'Donnell, K.; Thomsen, L.; Hodgkiss, J. M.; Watkins, S. E.; McNeill, C. R., Performance, Morphology and Photophysics of High Open-Circuit Voltage, Low Band Gap All-Polymer Solar Cells. *Energy Environ. Sci.* **2015,** *8*, 332-342.
36. Bi, P.; Hao, X., Versatile Ternary Approach for Novel Organic Solar Cells: A Review. *Sol. RRL* **2019,** *3*, 1800263.
37. Wang, Z.; Zhu, X.; Zhang, J.; Lu, K.; Fang, J.; Zhang, Y.; Wang, Z.; Zhu, L.; Ma, W.; Shuai, Z. et al., From Alloy-Like to Cascade Blended Structure: Designing High-Performance All-Small-Molecule Ternary Solar Cells. *J. Am. Chem. Soc.* **2018,** *140*, 1549-1556.
38. An, Q.; Zhang, F.; Yin, X.; Sun, Q.; Zhang, M.; Zhang, J.; Tang, W.; Deng, Z., High-Performance Alloy Model-Based Ternary Small Molecule Solar Cells. *Nano Energy* **2016,** *30*, 276-282.
39. Zhang, J.; Zhang, Y.; Fang, J.; Lu, K.; Wang, Z.; Ma, W.; Wei, Z., Conjugated Polymer–Small Molecule Alloy Leads to High Efficient Ternary Organic Solar Cells. *J. Am. Chem. Soc.* **2015,** *137*, 8176-8183.
40. Proctor, C. M.; Kim, C.; Neher, D.; Nguyen, T.-Q., Nongeminate Recombination and Charge Transport Limitations in Diketopyrrolopyrrole-Based Solution-Processed Small Molecule Solar Cells. *Adv. Funct. Mater.* **2013,** *23*, 3584-3594.
41. Ran, N. A.; Love, J. A.; Heiber, M. C.; Jiao, X.; Hughes, M. P.; Karki, A.; Wang, M.; Brus, V. V.; Wang, H.; Neher, D. et al., Charge Generation and Recombination in an Organic Solar Cell with Low Energetic Offsets. *Adv. Energy Mater.* **2018,** *8*, 1701073.
42. Baran, D.; Kirchartz, T.; Wheeler, S.; Dimitrov, S.; Abdelsamie, M.; Gorman, J.; Ashraf, R. S.; Holliday, S.; Wadsworth, A.; Gasparini, N. et al., Reduced Voltage Losses Yield 10% Efficient Fullerene Free Organic Solar Cells with >1 V Open Circuit Voltages. *Energy Environ. Sci.* **2016,** *9*, 3783-3793.
43. Zhang, G.; Zhang, K.; Yin, Q.; Jiang, X.-F.; Wang, Z.; Xin, J.; Ma, W.; Yan, H.; Huang, F.; Cao, Y., High-Performance Ternary Organic Solar Cell Enabled by a Thick Active Layer Containing a Liquid Crystalline Small Molecule Donor. *J. Am. Chem. Soc.* **2017,** *139*, 2387-2395.
44. Jiang, K.; Zhang, G.; Yang, G.; Zhang, J.; Li, Z.; Ma, T.; Hu, H.; Ma, W.; Ade, H.; Yan, H., Multiple Cases of Efficient Nonfullerene Ternary Organic Solar Cells Enabled by an Effective Morphology Control Method. *Adv. Energy Mater.* **2018,** *8*, 1701370.
45. Li, W.; Yan, Y.; Gong, Y.; Cai, J.; Cai, F.; Gurney, R. S.; Liu, D.; Pearson, A. J.; Lidzey, D. G.; Wang, T., Contrasting Effects of Energy Transfer in Determining Efficiency Improvements in Ternary Polymer Solar Cells. *Adv. Funct. Mater.* **2018,** *28*, 1704212.
46. Li, W.; Chen, M.; Cai, J.; Spooner, E. L. K.; Zhang, H.; Gurney, R. S.; Liu, D.; Xiao, Z.; Lidzey, D. G.; Ding, L. et al., Molecular Order Control of Non-fullerene Acceptors for High-Efficiency Polymer Solar Cells. *Joule* **2019,** *3*, 819-833.
47. Wu, W.-R.; Jeng, U. S.; Su, C.-J.; Wei, K.-H.; Su, M.-S.; Chiu, M.-Y.; Chen, C.-Y.; Su, W.-B.; Su, C.-H.; Su, A.-C., Competition between Fullerene Aggregation and Poly(3-hexylthiophene) Crystallization upon Annealing of Bulk Heterojunction Solar Cells. *ACS Nano* **2011,** *5*, 6233-6243.
48. Liao, H.-C.; Tsao, C.-S.; Lin, T.-H.; Chuang, C.-M.; Chen, C.-Y.; Jeng, U. S.; Su, C.-H.; Chen, Y.-F.; Su, W.-F., Quantitative Nanoorganized Structural Evolution for a High Efficiency Bulk Heterojunction Polymer Solar Cell. *J. Am. Chem. Soc.* **2011,** *133*, 13064-13073.
49. Huang, Y.-C.; Tsao, C.-S.; Chuang, C.-M.; Lee, C.-H.; Hsu, F.-H.; Cha, H.-C.; Chen, C.-Y.; Lin, T.-H.; Su, C.-J.; Jeng, U. S. et al., Small- and Wide-Angle X-ray Scattering Characterization of Bulk Heterojunction Polymer Solar Cells with Different Fullerene Derivatives. *J. Phys. Chem. C* **2012,** *116*,

10238-10244.

50. Chiu, M.-Y.; Jeng, U. S.; Su, C.-H.; Liang, K. S.; Wei, K.-H., Simultaneous Use of Small- and Wide-Angle X-ray Techniques to Analyze Nanometerscale Phase Separation in Polymer Heterojunction Solar Cells. *Adv. Mater.* **2008,** *20*, 2573-2578.

51. Jin, F.; Yuan, J.; Guo, W.; Xu, Y.; Zhang, Y.; Sheng, C.; Ma, W.; Zhao, H., Improved Charge Generation via Ultrafast Effective Hole-Transfer in All-Polymer Photovoltaic Blends with Large Highest Occupied Molecular Orbital (HOMO) Energy Offset and Proper Crystal Orientation. *Adv. Funct. Mater.* **2018,** *28*, 1801611.

52. Österbacka, R.; An, C. P.; Jiang, X. M.; Vardeny, Z. V., Two-Dimensional Electronic Excitations in Self-Assembled Conjugated Polymer Nanocrystals. *Science* **2000,** *287*, 839.

53. Tamai, Y.; Tsuda, K.; Ohkita, H.; Benten, H.; Ito, S., Charge-Carrier Generation in Organic Solar Cells Using Crystalline Donor Polymers. *Phys. Chem. Chem. Phys.* **2014,** *16*, 20338-20346.

54. Yin, H.; Bi, P.; Cheung, S. H.; Cheng, W. L.; Chiu, K. L.; Ho, C. H. Y.; Li, H. W.; Tsang, S. W.; Hao, X.; So, S. K., Balanced Electric Field Dependent Mobilities: A Key to Access High Fill Factors in Organic Bulk Heterojunction Solar Cells. *Sol. RRL* **2018,** *2*, 1700239.

55. Ho, C. H. Y.; Cheung, S. H.; Li, H.-W.; Chiu, K. L.; Cheng, Y.; Yin, H.; Chan, M. H.; So, F.; Tsang, S.-W.; So, S. K., Using Ultralow Dosages of Electron Acceptor to Reveal the Early Stage Donor–Acceptor Electronic Interactions in Bulk Heterojunction Blends. *Adv. Energy Mater.* **2017,** *7*, 1602360.

56. Lee, H. K. H.; Li, Z.; Constantinou, I.; So, F.; Tsang, S. W.; So, S. K., Batch-to-Batch Variation of Polymeric Photovoltaic Materials: its Origin and Impacts on Charge Carrier Transport and Device Performances. *Adv. Energy Mater.* **2014,** *4*, 1400768.

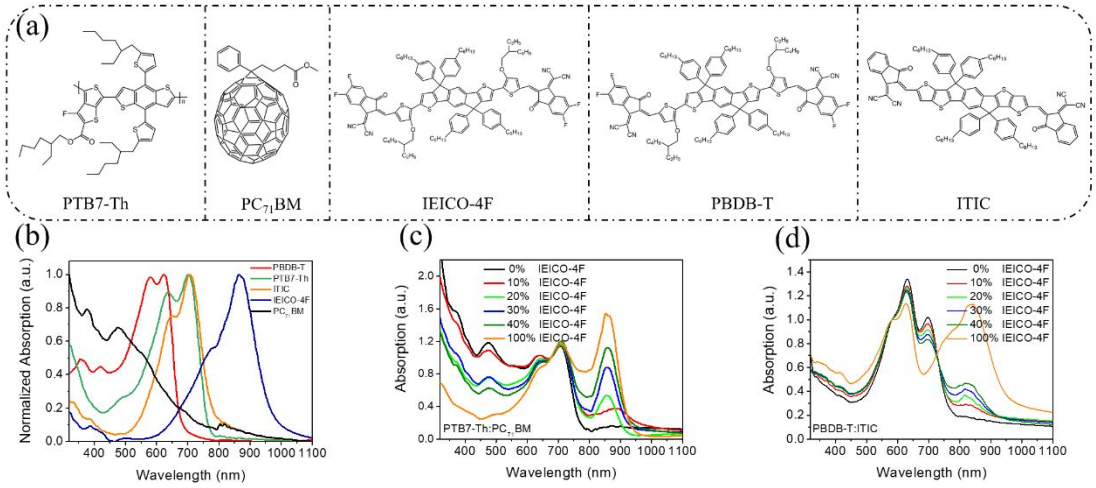

Figure 1. (a) Material chemical structures. (b) Normalized UV–Vis absorption spectra of neat films. (c) Absorption spectra of PTB7-Th: IEICO-4F: $PC_{71}BM$ with various doping ratios of IEICO-4F, and (d) PBDB-T: IEICO-4F: ITIC with various doping ratios of IEICO-4F (Normalized at 676 nm).

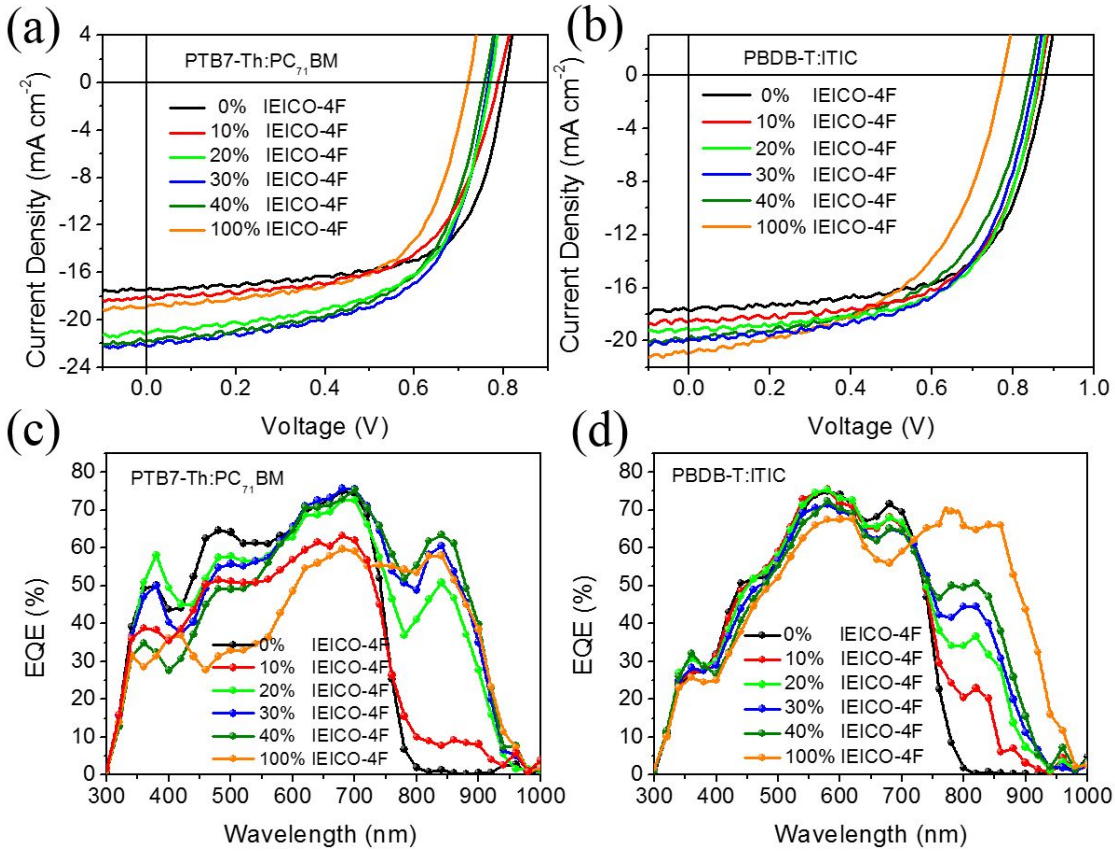

Figure 2. *J–V* and EQE curves of (a, c) PTB7-Th: IEICO-4F: $PC_{71}BM$ with various amounts of IEICO-4F and (b, d) PBDB-T: IEICO-4F: ITIC with different amounts of IEICO-4F.

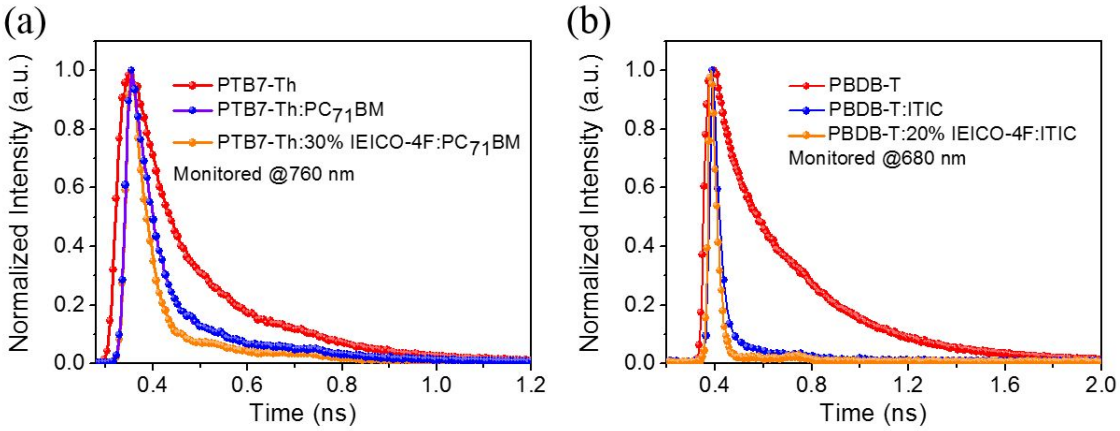

Figure 3. Normalized fluorescence decay kinetics of (a) PTB7-Th in neat and blend films, (b) PBDB-T in neat and blend films.

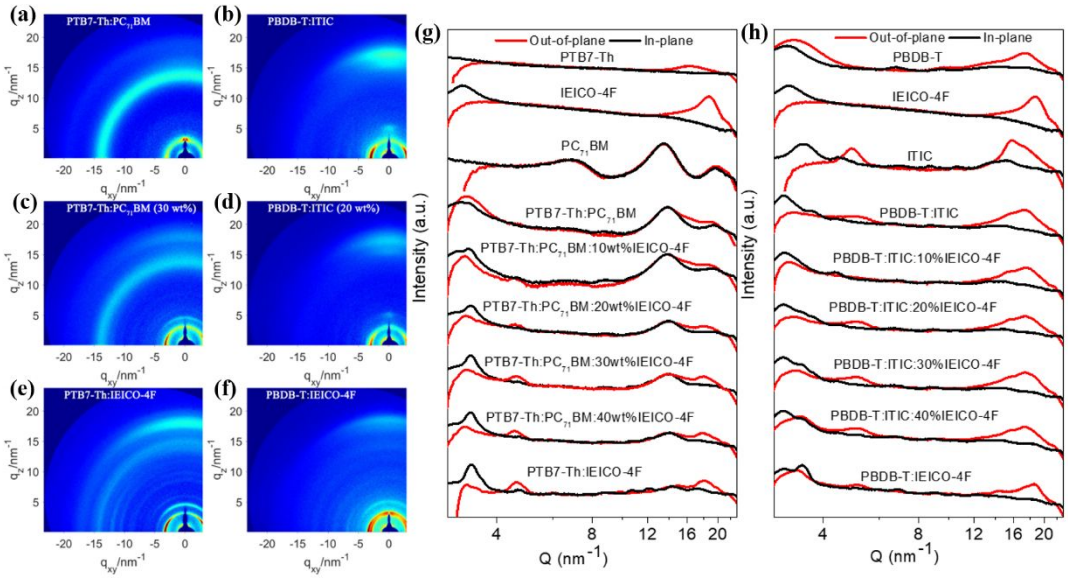

Figure 4. (a)-(f) 2D GIWAXS patterns of the blends films and the corresponding out-of-plane and in-plane profiles of GIWAXS patterns of (g) PTB7-Th:$PC_{71}BM$ system and (h) PBDB-T:ITIC system.

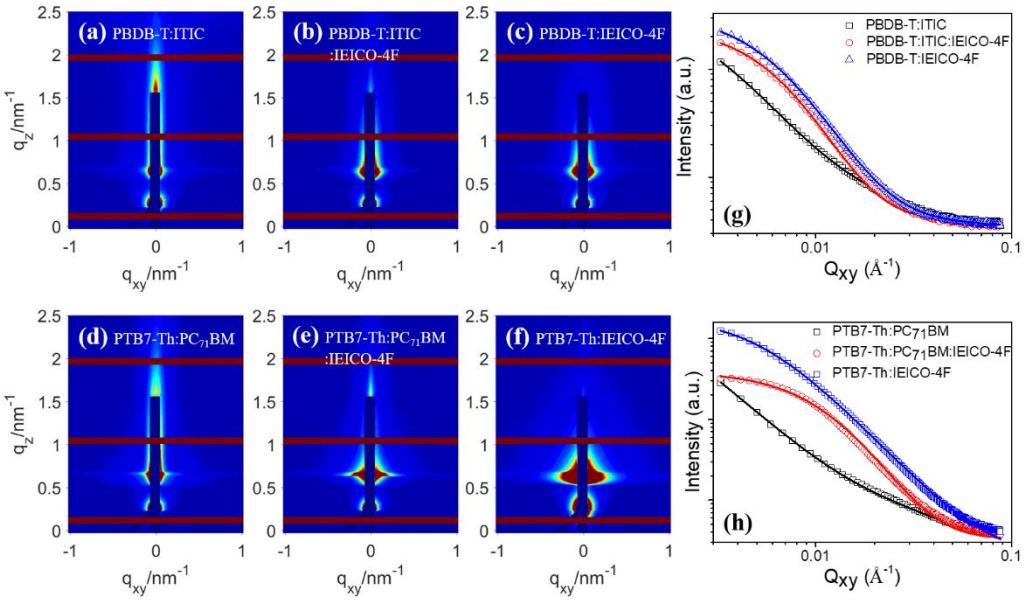

Figure 5. 2D GISAXS scattering patterns of binary and ternary films (a-c) PBDB-T:ITIC based systems (d-f) PTB7-Th:$PC_{71}BM$ based systems and (g) (h) in-plane profiles of each film.

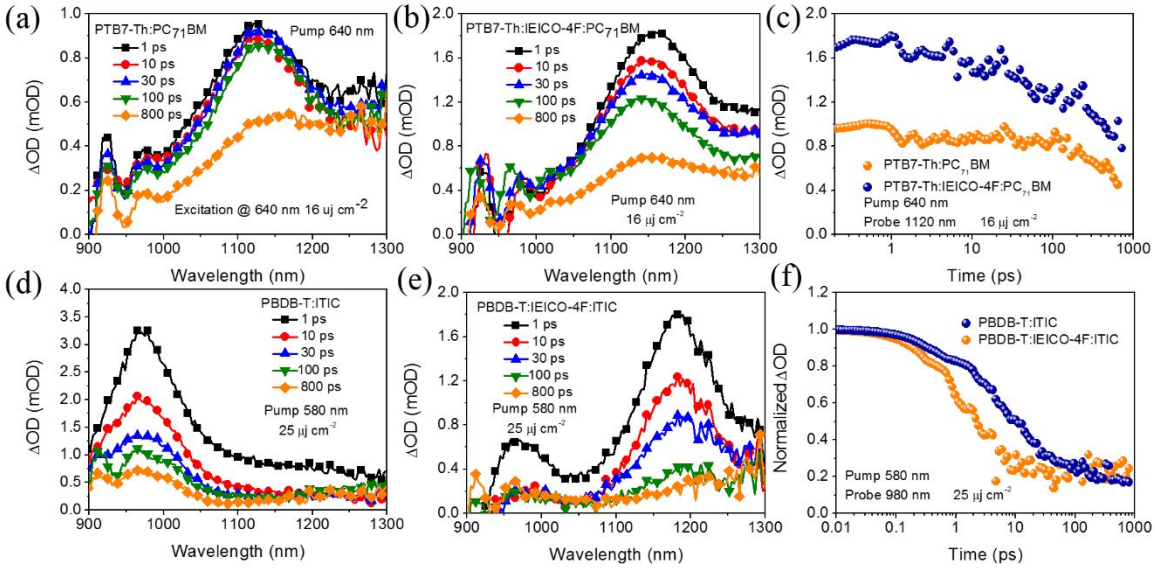

Figure 6. TA spectra of (a) PTB7-Th:$PC_{71}BM$, (b) PTB7-Th:IEICO-4F:$PC_{71}BM$, (d) PBDB-T:ITIC, (e) PBDB-T:IEICO-4F:ITIC, and decay kinetics of the (c) PTB7-Th:$PC_{71}BM$-based system and (f) PBDB-T:ITIC system.

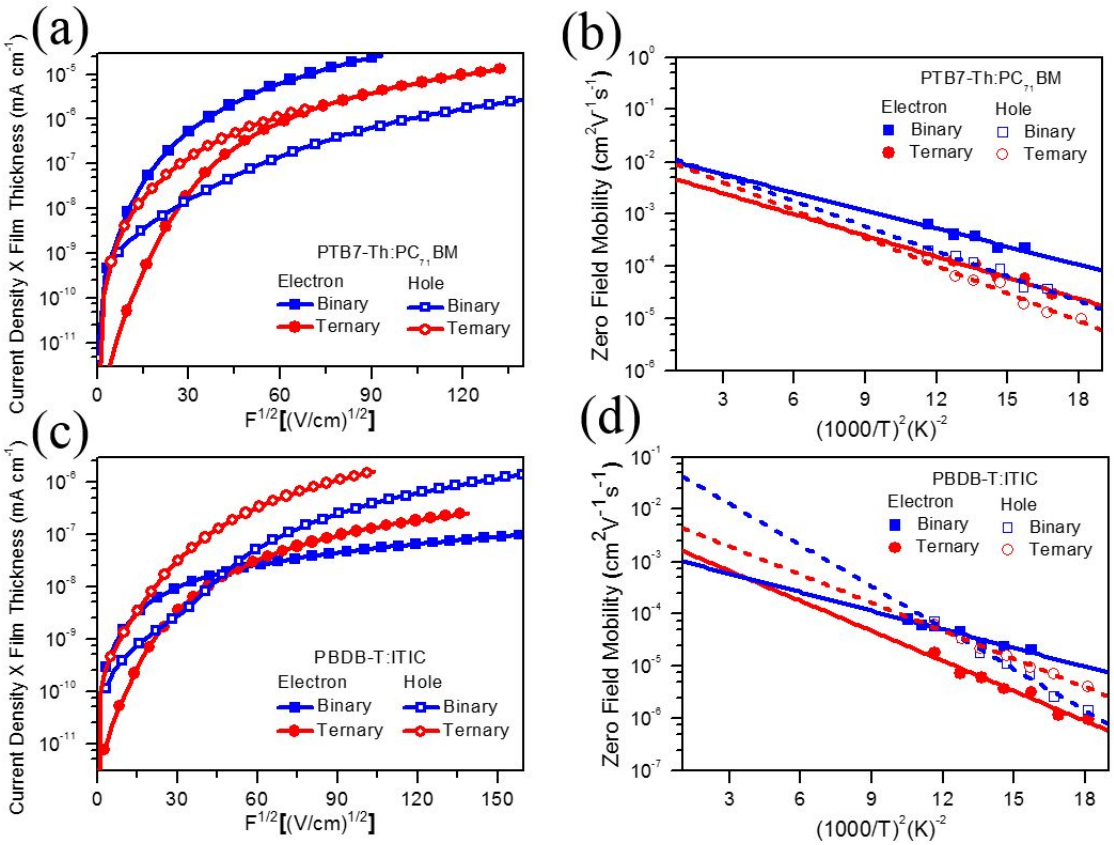

Figure 7. Transport data of binary and ternary with hole-only and electron-only devices. (a) *J–V* data and SCLC fittings at room temperature in the semi-log plot and zero-field mobility against $1/T^2$ for the GDM analysis of (a, b) PTB7-Th:$PC_{71}BM$ system and (c, d) PBDB-T:ITIC system.

Table 1. Ternary OSC properties based on PTB7-Th:$PC_{71}BM$ and PBDB-T:ITIC.

Materials	V_{OC} (V)	J_{SC} (mA cm^{-2})	FF	PCE_{ave} (%)	PCE_{max} (%)
PTB7-Th:$PC_{71}BM$	0.80	17.39	0.65	9.07	9.16
With 10% IEICO-4F	0.78	18.03	0.61	8.56	8.70
With 20% IEICO-4F	0.77	20.63	0.62	9.63	9.94
With 30% IEICO-4F[a)]	0.76	22.97	0.61	10.43	10.76
With 30% IEICO-4F[b)]	0.77	23.68	0.61	11.06	11.24
With 40% IEICO-4F	0.75	21.77	0.60	9.62	9.78
With 100% IEICO-4F	0.72	18.85	0.61	8.02	8.33
PBDB-T:ITIC	0.87	17.13	0.62	9.16	9.26
With 10% IEICO-4F	0.86	18.54	0.62	9.70	9.98
With 20% IEICO-4F	0.86	19.14	0.62	10.08	10.25
With 30% IEICO-4F	0.85	19.89	0.59	9.78	10.16
With 40% IEICO-4F	0.84	19.81	0.57	9.34	9.69
With 100% IEICO-4F	0.77	20.91	0.52	8.13	8.50

[a)]With 3 vol% DIO in the blends. [b)]With 1.5 vol% DIO in the blends.

Table 2. Transport parameters extracted from SCLC fitting and GDM analysis.

			μ_0 ($cm^2V^{-1}s^{-1}$)	σ (meV)
PBDB-T:ITIC	Electron	Binary	5.95×10^{-5}	68
		Ternary	1.82×10^{-5}	86
	Hole	Binary	6.94×10^{-5}	101
		Ternary	6.22×10^{-5}	82
PTB7-Th:$PC_{71}BM$	Electron	Binary	6.43×10^{-4}	66
		Ternary	1.53×10^{-4}	72
	Hole	Binary	2.02×10^{-4}	78

	Ternary	1.31×10^{-4}	82

TOC